



1 **Morphology, mixing state, and hygroscopicity of primary biological**  
2 **aerosol particles from a Chinese boreal forest**

3

4 Weijun Li<sup>1</sup>, Lei Liu<sup>1</sup>, Qi Yuan<sup>1</sup>, Liang Xu<sup>1</sup>, Yanhong Zhu<sup>1</sup>, Bingbing Wang<sup>2</sup>, Hua Yu<sup>3</sup>, Xiaokun

5 Ding<sup>4</sup>, Jian Zhang<sup>1</sup>, Dao Huang<sup>1</sup>, Dantong Liu<sup>1</sup>, Wei Hu<sup>5</sup>, Daizhou Zhang<sup>6</sup>, Pingqing Fu<sup>5</sup>,

6 Maosheng Yao<sup>7</sup>, Min Hu<sup>7</sup>, Xiaoye Zhang<sup>8</sup>, Zongbo Shi<sup>9,5</sup>

7 <sup>1</sup>Department of Atmospheric Sciences, School of Earth Sciences, Zhejiang University, Hangzhou

8 310027, China

9 <sup>2</sup>State Key Laboratory of Marine Environmental Science, College of Ocean and Earth Sciences,

10 Xiamen University, Xiamen 361102, China.

11 <sup>3</sup>College of Life and Environmental Sciences, Hangzhou Normal University, 310036, Hangzhou, China

12 <sup>4</sup>Department of Chemistry, Zhejiang University, Hangzhou 310027, China

13 <sup>5</sup>Institute of Surface-Earth System Science, Tianjin University, 300072, Tianjin, China

14 <sup>6</sup>Faculty of Environmental and Symbiotic Sciences, Prefectural University of Kumamoto,

15 Kumamoto 862-8502, Japan

16 <sup>7</sup>State Key Joint Laboratory of Environmental Simulation and Pollution Control, College of

17 Environmental Sciences and Engineering, Peking University, Beijing 100871, China

18 <sup>8</sup>Key Laboratory of Atmospheric Chemistry, Chinese Academy of Meteorological Sciences, Beijing,

19 China

20 <sup>9</sup>School of Geography, Earth and Environmental Sciences, University of Birmingham,

21 Birmingham B15 2TT, UK

22 \*Correspondence to: Weijun Li (liweijun@zju.edu.cn)



23 **Abstract:**

24 Biological aerosols play an important role in atmospheric chemistry, clouds, climate, and public  
25 health. Here, we studied the morphology and composition of primary biological aerosol particles  
26 (PBAPs) collected in the Lesser Khingan Mountain boreal forest of China in summertime using  
27 transmission electron microscopy and scanning electron microscopy. Of all detected particles >  
28 100 nm in diameter, 13% by number were identified as PBAPs. In addition, 57% of the PBAPs  
29 were identified as bacteria, followed by brochosomes (24%) and fungi (19%). The dominant size  
30 of bacteria was 1-4  $\mu\text{m}$ , fungi was 2-4  $\mu\text{m}$ , and brochosomes was 300-500 nm. The number size  
31 distribution of PBAPs coupled with the mass concentrations of  $\text{PM}_{2.5}$  and  $\text{PM}_{10}$  were used to  
32 estimate the total mass concentration of PBAPs, which is approximately  $1.9 \mu\text{g m}^{-3}$  and accounts  
33 for 47% of the in situ  $\text{PM}_{2.5-10}$  mass. C, N, O, P, K, and Si are detected in all PBAP particles, and P  
34 represented a major marker to identify PBAPs. Moreover, there is a higher frequency and  
35 concentration of PBAPs at night compared with day. Bacterial and fungal particles displayed weak  
36 hygroscopicity with a growth factor of  $\sim 1.09$  at  $\text{RH}=94\%$ . Electron microscopy shows that  
37 approximately 20% of the bacterial particles were internally mixed with metal, mineral dust, and  
38 inorganic salts in the boreal forest air. This work provides a database for both further  
39 understanding physicochemical state of individual PBAP particles from natural sources and  
40 expanding the scope of atmospheric implications.

41

42



43 **Key points**

44

45 • In a boreal forest, 57% of the PBAPs were identified as bacteria, 19% as fungi and 24% as  
46 brochosomal particles.

47 • Emissions of PBAPs tend to occur with high humidity at night rather than during the day.

48 • Hygroscopic experiments show that most of the primary PBAPs displayed weak  
49 hygroscopicity, and their growth factor was  $\sim 1.09$  at RH=94%.

50



## 51 **1. Introduction**

52 Primary biological aerosol particles (PBAPs) (e.g., bacteria, spores, fungi, viruses, algae, and  
53 pollen) are ubiquitous in the Earth's atmosphere and represent key elements in the life cycle of  
54 many organisms and ecosystems (Poschl, 2005; Tunved et al., 2006). PBAPs are airborne  
55 biological materials that prevail from the biosphere to the atmosphere (Huffman et al., 2010), and  
56 they can account for a large proportion of the aerosol particle mass in pristine forest air as well as  
57 in some rural and ocean environments (Elbert et al., 2007; Bauer et al., 2008; Hu et al., 2017; May  
58 et al., 2018). Research interest in biological aerosol has been growing significantly in recent  
59 decades (Després et al., 2012). Laboratory studies have shown that certain cell fragments in  
60 biological aerosols may be active as both cloud condensation nuclei (CCN) and ice nuclei (IN)  
61 (Morris et al., 2004; Ling et al., 2018). A recent study demonstrated that fungal spores emitted by  
62 the forest contain abundant sodium salt particles in the central Amazon basin and significantly  
63 influence the hygroscopicity and CCN of PBAPs (China et al., 2018). Furthermore, field  
64 campaigns have found that abundant biological aerosols occur in cloud ice-crystals, fog/cloud,  
65 rain, and snowfall (Amato et al., 2005; Möhler et al., 2007; Christner et al., 2008; Pratt et al.,  
66 2009; Twohy et al., 2016; Hu et al., 2018). These studies addressed the hypothesis that PBAPs  
67 indeed influence the hydrological cycle and climate by initiating the formation of clouds and  
68 precipitation as CCN and IN. PBAPs in pristine regions significantly contribute to the particle  
69 mass and number and have important implications for radiation budget estimates in the  
70 atmosphere (Tunved et al., 2006; Martin et al., 2010; Tobo et al., 2013). Although PBAPs only have  
71 a small contribution to particulate mass in polluted urban air, pollen and spores from plants can  
72 induce human allergic symptoms worldwide (Denning et al., 2006; Zhou et al., 2019).



73 Previous studies have investigated the sampling, particle number concentration, shape, and  
74 chemical characterization of primary biological aerosols (Wittmaack et al., 2005; Elbert et al.,  
75 2007; Fröhlich-Nowoisky et al., 2009; Huffman et al., 2010; Després et al., 2012; Hu et al.,  
76 2017; Therkorn et al., 2017; Zhang et al., 2017; Chen and Yao, 2018). For example, the contribution  
77 of fungal spores to total organic carbon was estimated to be approximately 10% in clean and  
78 polluted periods in Beijing (Yue et al., 2017) and 0.9% (up to 9.9% in coarse size) in the Austrian  
79 Alps (Bauer et al., 2002). Elbert et al. (2007) reported that the mean mass concentration of PBAPs  
80 was  $\sim 1 \mu\text{g m}^{-3}$  and accounted for 20% of total coarse particle mass in central Europe. To obtain the  
81 chemical composition of PBAPs, many studies tend to detect biochemical markers (e.g., proteins,  
82 fatty acids, sugars) and nucleic acids (i.e., DNA and RNA) to determine their properties in the  
83 atmosphere (Georgakopoulos et al., 2009; Chen and Yao, 2018; Hu et al., 2018; Ling et al., 2018).  
84 These comprehensive and detailed studies of time- and size-resolved PBAPs and their biochemical  
85 markers do not well explain the physical properties (e.g., morphology, phase, hygroscopicity, and  
86 mixing state) of individual PBAPs in the atmosphere

87 A limited number of studies have provided detailed morphological and mixing state data on  
88 PBAPs (Posfai et al., 2003; Wittmaack, 2005; Wittmaack et al., 2005; China et al., 2018).  
89 Information on the morphology, size, and mixing state of different PBAPs allow for the  
90 identification of biological particle types and provide insights into the actual state of individual  
91 biological particles suspended in the atmosphere (Posfai et al., 2003; Wittmaack et al., 2005; Martin  
92 et al., 2010; Després et al., 2012). Single particle analyses can characterize the physical and  
93 chemical properties of individual particles from the nanoscale to microscale (Li et al., 2016), and  
94 this approach can also indicate the optical and hygroscopic properties and possible sources of



95 these particles. Thus far, only a few studies have observed the morphology and size of some  
96 biological aerosols via scanning electron microscopy (SEM) (Shi et al., 2003;Wittmaack et al.,  
97 2005;Shi et al., 2009;Martin et al., 2010;Huffman et al., 2012;Valsan et al., 2015;Wu et al., 2019).  
98 For example, fungal fragments sampled from Amazonia contain hygroscopic sodium salts based  
99 on an environmental scanning electron microscopy (ESEM) analysis, and these salts significantly  
100 influence the hygroscopic growth and light scattering of the fragments (China et al., 2016;China et  
101 al., 2018). However, whether fungal spores emitted by boreal forests are similar to the fungal  
102 spores in central Amazon forests, which contain sodium salts, has not been resolved. Therefore,  
103 the morphology, elemental composition, and mixing state of individual PBAPs (nanometer to  
104 micrometer size) collected from other global forests must be analyzed.

105 Forests are important contributors of primary biological aerosols in the atmosphere (Tunved et  
106 al., 2006;Spracklen et al., 2008;Després et al., 2012). Aerosols in large forests contain abundant  
107 biological particles from plants and lesser anthropogenic pollutants of long-range transport  
108 (Tunved et al., 2006;Gabey et al., 2010;Martin et al., 2010). We chose the Lesser Khingan  
109 Mountains in Northeast China, which is the second largest boreal forest in China. In this study,  
110 integrated single-particle techniques are required to clearly observe individual PBAPs from the  
111 nanoscale to microscale and further reveal their hygroscopicity in the atmosphere. Transmission  
112 electron microscopy (TEM) and scanning electron microscopy (SEM) both have been employed to  
113 characterize the morphology, size, and mixing state of various PBAPs collected over the boreal  
114 forest. Furthermore, hygroscopic experiments on the primary biological particles have been  
115 conducted.

116



117 **2. Methods**

118 **2.1 Sampling site and sample collection**

119 The sampling site is at the Heilongjiang Liangshui National Nature Reserve (47.32° N,  
120 128.54° E) in the center of the Lesser Khingan Mountains of Northeast China (Figure 1). The  
121 boreal region is characterized by large seasonal variations in temperature, and the flora is  
122 dominated by Korean pine and spruce species. There are no anthropogenic sources of pollutants,  
123 such as villages, industries and vehicles within 80 km of the sampling site. Because boreal forests  
124 play a key role in biological aerosol emissions during summer, we collected aerosol samples in  
125 August.

126 Aerosol particles were collected on copper (Cu) grids coated with a carbon (C) film (carbon  
127 type-B, 300-mesh copper, Tianld Co., China) and silicon wafer by a DKL-2 sampler (Jenstar  
128 Electronic Technology, China) with a single-stage cascade impactor (Li and Shao, 2009) equipped  
129 with a 0.5 mm diameter jet nozzle at a flow rate of 1.0 L/min at 9:00, 15:00, 21:00, and 2:00 a.m.  
130 (midnight) local time every day. The sampling duration at each time varied from 10 min to 25 min  
131 depending on the particle distribution on the substrate. After sample collection, we immediately  
132 performed optical microscopy at 100 magnification to determine whether the aerosol distribution  
133 on the substrate was suitable for electron microscopy analysis. The sampling procedure can  
134 guarantee that the collected particles separated or did not overlap each other on the substrate (Li et  
135 al., 2016). The collection efficiency of the impactor is 50% for particles with an aerodynamic  
136 diameter of 0.1  $\mu\text{m}$  when we assume an aerosol particle density of 2  $\text{g cm}^{-3}$ . The Cu grids and  
137 silicon wafers placed in a dry, clean, and airtight container were stored in a desiccator at 25 °C and  
138 20±3% RH to minimize exposure to ambient air and preserve them for analysis.



139 The daily PM<sub>2,5</sub> and PM<sub>10</sub> samples were collected on quartz-fiber filters with a diameter at 90  
140 mm through two medium-volume samplers (TH-150, Wuhan Tianhong, China) at a constant flow  
141 rate of 100 L min<sup>-1</sup>. The samples were changed at 08:00 a.m. each day. Our sampling and  
142 monitoring instruments in the field experiment were installed on a building roof 15 m above  
143 ground. The quartz filters were put in polyethylene boxes immediately after sampling and stored  
144 at -5 °C. The filters were equilibrated at a constant temperature (20 ± 0.5 °C) and humidity (50 ±  
145 2%) for over 24 h before being weighed with an electronic microbalance (Sartorius-ME5,  
146 Germany). Meteorological data, including the relative humidity (RH), temperature, wind speed,  
147 and wind direction, were measured and recorded every 5 min by an automated weather meter  
148 (Kestrel 5500, USA). During the sampling period, the relative humidity (RH) and temperature  
149 varied from 40-70% and 22-28 °C during the day and 90-100% and 10-15 °C during the night,  
150 respectively. The wind speed was 1.5-7.6 m s<sup>-1</sup> during the day and 0-1 m s<sup>-1</sup> at night (Figure S1).

## 151 2.2 Transmission electron microscopy analysis

152 Individual aerosol particles collected on Cu grids were analyzed via transmission electron  
153 microscopy (TEM, JEM-2100, JEOL Ltd., Japan) at a 200 kV accelerating voltage. The TEM  
154 system is equipped with an energy-dispersive X-ray spectrometer (EDS, INCA X-Max<sup>N</sup> 80T,  
155 Oxford Instruments, UK). EDS semiquantitatively detects the elemental composition of individual  
156 particles with an atomic number greater than six ( $Z > 6$ ). However, Cu peaks in the EDS spectra  
157 were not considered because of interference from the copper substrate of TEM grids. We  
158 determined the morphology, composition, and mixing state of individual particles through the  
159 combination of TEM and EDS. To reduce the damage to particles under the electron beam, the  
160 EDS collection duration was limited to 15 s. Particles in 3-5 grids of each sample were analyzed to



161 ensure their universality and representativeness. TEM can determine the internal mixing structure  
162 of different aerosol components in fine particles and their specific composition.

### 163 **2.3 Scanning electron microscopy analysis**

164 Scanning electron microscopy (SEM) is performed using a type of electron microscope that  
165 can determine the particle surface by scanning it with a high-energy beam of electrons in a raster  
166 scan pattern. An SEM system (Zeiss Ultra 55) equipped with a field emission gun operating at 5–  
167 20 kV was used to obtain detailed information on the surfaces of individual aerosol particles.  
168 Moreover, the SEM was equipped with an energy-dispersive X-ray spectrometry (EDS), which  
169 can analyze the chemical composition of individual particles. The SEM can efficiently obtain the  
170 surface morphology, size, and composition of coarse particles without any coating process on the  
171 substrate.

### 172 **2.4 Hygroscopic experiments**

173 A custom-made individual particle hygroscopic (IPH) system was used to observe the  
174 hygroscopic properties of individual biological particles at different relative humidity (RH)  
175 values. The IPH system involved three steps: (1) introducing N<sub>2</sub> gas with a mass flow  
176 controller into a chamber; (2) setting a TEM grid or silicon wafer on the bottom of an  
177 environmental microscopic cell (Gen-RH Mcell, UK), which can change the RH and maintain  
178 the temperature at 20 °C; and (3) taking images at incremental RH values using an optical  
179 microscope (Olympus BX51M, Japan) with a camera (Canon 650D). This IPH system has  
180 successfully captured the hygroscopic growth of individual particles collected on either a  
181 silicon wafer or TEM grid (Sun et al., 2018). In this study, one typical sample containing  
182 biological particles was chosen to observe the hygroscopic growth of the bacterial and fungal



183 particles at RH values ranging from 5% to 94%. The particle growth factor (GF) is an  
184 important parameter used to describe the hygroscopic growth of individual particles, and it is  
185 defined as follows:

$$GF(RH) = \frac{D(RH)}{D_0}$$

186 where  $D(RH)$  and  $D_0$  are the diameters of particles at a given RH and at 5% RH, respectively.

187

### 188 3. Results and Discussion

#### 189 3.1 Morphology and elemental composition of PBAPs

190 Among the 4422 analyzed aerosol particles with diameters of 100 nm-10  $\mu\text{m}$ , individual  
191 particles are classified into five groups based on their morphology and composition: S-OM  
192 (mixture of sulfate (S), organics (OM)), OM, mineral dust, and PBAPs (Figure 2). S can be used  
193 to indicate secondary sulfates; abundant C and minor O with transparent color constitute the  
194 coating of the sulfate core and represent secondary organic matter; and irregular particles  
195 containing Si, Al, Ca and minor Fe, Ti normally indicate mineral dust particles. Moreover,  
196 previous studies have stated that elemental P in individual particles and the associated unique  
197 morphologies can be used to identify PBAPs via electron microscopy (Poschl, 2005; Wittmaack et  
198 al., 2005). Thirteen percent of particles were PBAPs, and low magnification SEM and TEM  
199 images both revealed that abundant PBAPs occurred in the samples (Figure 2a-d).

200 The number fractions of size-resolved aerosol particles show that secondary S-OM and OM  
201 particles were the dominant particle groups in the fine mode ( $< 1 \mu\text{m}$ ) while PBAPs and mineral  
202 particles dominated the coarse mode ( $\geq 1 \mu\text{m}$ ) (Figure 3a). Moreover, we noticed that the number  
203 fractions of PBAPs in each sample collected at night were much higher than those collected



204 during the day. Abundant fine secondary sulfate and organic particles from photochemical  
205 formation were observed during the day. Figure 3b shows that the average number fraction of  
206 PBAPs was 2.5% in the samples collected during the day and as high as 30.0% at night. If we  
207 further calculated the number concentration of PBAPs in Figure 3b, the PBAPs concentration  
208 significantly increased by approximately 7 times from daytime to nighttime, although the  
209 non-PBAPs concentration decreased.

210 The PBAPs were classified based on morphology into four types: bacterial, fungal,  
211 brochosomal, and other biological particles. Pollen was not found in our samples, which may be  
212 because large pollen emissions occur in spring and early summer instead of late summer (August).  
213 Similarly, Wittmaack et al. (2005) did not find pollen in the boreal forest air in other locations in  
214 late summer.

215 **Bacterial particles.** Figure 4 shows the typical morphology of the bacteria particles, which  
216 have a rod-like shape and include several dark inclusions (Posfai et al., 2003). These bacteria  
217 particles were stable under the electron beam during the TEM analysis, and they contained C, N,  
218 O, P, and K with minor Mg, Si, S, Ca and Fe (Figure 4). EDS further showed that the bacterial  
219 inclusions contained much higher P, Mg, and K while other parts contained much higher C, N, and  
220 O (Figure 4). Bacterial inclusions resemble a nucleoid and plasmid and other parts of the  
221 cytoplasm.

222 Figure 2b shows an SEM image of a bacterium particle and indicates its morphology  
223 (although no information about the inner structure is obtained). The surface of the bacterial  
224 particles is uneven and the surface contains clear wrinkles, which probably formed as the bacteria  
225 dried on the substrate (Patterson et al., 2016). Most of the bacterial particles have a rod-like shape



226 (Figure 5), and some showed a near-spherical shape (Figure 5). A majority of the individual  
227 bacteria particles is present as a single bacteria cell, although some form aggregates (Figure 2a, c).

228 **Fungal particles.** SEM images show that various fungal particles occurred in the boreal  
229 forest air (Figure 2a). TEM observations show that the fungal particles generally display irregular  
230 shapes and rough surfaces and that they mainly contain C, O and Si and following minor N, Mg, P,  
231 S, K and Fe (Figure 6). Figure 6 shows that several typical fungal particles with diameters of  
232 3.7-6.5  $\mu\text{m}$  do not have well-defined shapes and their surfaces have regular strips or regular  
233 bubble. Based on the classifications of fungal particles from Wittmaack et al. (2005), particles  
234 shown in Figures 6a and 7a-d and in Figures 6b-c and 7e-f were considered as conidia and spores,  
235 respectively.

236 We identified 19% of the primary biological particles as fungi in this study. Compared with  
237 bacterial particles, fungal particles normally have a rougher surface (Figures 6-7) and contain  
238 much higher Si and lower N. Moreover, a few fungal particles are found associated with fragments  
239 of other unknown biological particles (Figures 7a, d, e).

240 **Brochosomal particles.** TEM observations show that brochosomal particles frequently  
241 occurred in the samples and accounted for 24% of the analyzed primary biological particles.  
242 Interestingly, the outline of each brochosome approximates a truncated icosahedron and the  
243 brochosome particles likely have unique inner structures, such as C<sub>60</sub> Buckminster fullerenes  
244 (Figures 8a-b and 9). Compared with the bacterial and fungal particles, the chemical compositions  
245 of the brochosomal particles show extremely high Si and low P in addition to major C and O and  
246 minor N, Na, S, K and Fe.

247 **Other biological particles.** In this study, we observed only a few elongated particles among



248 the biological particles. TEM observations show that these particles mainly contain C, O, and Si.  
249 It should be noted that P is not detectable in some of these biological particles as shown in Figures  
250 10-11. Because of the low particle numbers, we could not statistically determine their size  
251 distribution. The TEM and SEM images both show that these particles are quite large at 8-20  $\mu\text{m}$ .  
252 We speculate that these biological particles were fragments of plants or insects. For example,  
253 Wittmaack et al. (2005) suggested that the spaghetti-type biological particles from Figure 10a-d  
254 and Figure 11c are likely epicuticular wax fragments of plants. The biological particles with  
255 recognizable surface features from Figures 10e and 11a-b resemble part of insects. Because these  
256 biological particles are large, the TEM and SEM analyses both easily identified them, although the  
257 SEM analysis provided better and more detailed information of the large biological particles in the  
258 samples.

### 259 3.2 Relative abundance of PBAPs

260 Bacterial particles range from 400 nm to 10  $\mu\text{m}$ , with a peak diameter at 1-4  $\mu\text{m}$  (Figure 12a).  
261 Of the total analyzed primary biological particles, 57% were identified as bacterial particles  
262 (Figure 12a). Most fungal particles occurred in the coarse mode and their size distribution  
263 dominated at 2-4  $\mu\text{m}$  with one peak at 3  $\mu\text{m}$ . Brochosome particles dominate at 300-500 nm and  
264 have one main peak at 300 nm. SEM observations show that brochosomal particle clusters were  
265 distributed on the substrate (Figure 9a). This is because certain hygrophobic secretions of insects  
266 (e.g., leafhoppers) are composed of brochosomal particles, and these secretions function in  
267 keeping the insect cuticle dry (Wittmaack, 2005; Rakitov and Gorb, 2013).

268 Figure 12b shows the daily mass concentrations of  $\text{PM}_{2.5}$  at  $\sim 6 \mu\text{g m}^{-3}$  and  $\text{PM}_{10}$  at  $\sim 10 \mu\text{g m}^{-3}$   
269 and the ratio of  $\text{PM}_{2.5}/\text{PM}_{10}$  at  $\sim 0.6$  at the sampling site. The results from the electron microscopy



270 analysis further estimated that PBAPs, mineral dust, and the remaining particles accounted for  
271 50%, 25%, and 25% of the coarse mode, respectively (Figure 3a). Assuming a density of  $\sim 1$  g  
272  $\text{cm}^{-3}$  for PBAPs (Elbert et al., 2007),  $2$  g  $\text{cm}^{-3}$  for mineral dust particles, and  $1.4$  g  $\text{cm}^{-3}$  for the  
273 remaining particles (e.g., S-OM, OM, and metal) (Rissler et al., 2006), mass concentrations of  
274 three different types of particles with different size bins can be further calculated based on particle  
275 number and geometrical diameter as shown in Figure 3a. Finally, we can estimate that the mass  
276 concentration of PBAPs, mineral dust, and remaining particles accounted for 47%, 43%, and 10%  
277 of  $\text{PM}_{2.5-10}$ , respectively. The results suggest that large boreal forests are significant sources of  
278 PBAPs in summertime in Northeast China.

279 Thirteen percent of all detected particles collected from the boreal forest air are PBAPs. Such  
280 a high fraction of PBAPs has not been reported in urban and rural air in China (Shi et al., 2003; Shi  
281 et al., 2009; Li et al., 2016). The number concentration of PBAPs is higher at night than during the  
282 day (Figure 3b). A shallower nocturnal boundary layer will lead to an increase in the number  
283 concentration of coarse particles near the ground (Graham et al., 2003), although this increase  
284 cannot explain the very large difference in the relative number fraction of PBAPs (12 times larger  
285 at night than during the day) (Figure 3b). Therefore, this difference can only be explained by the  
286 higher relative emission strength of PBAPs compared with non-PBAPs or the differential removal  
287 of non-PBAPs. However, the latter is unlikely considering the usually larger size of non-PBAPs.

288 We compared the meteorological parameters (e.g., RH, temperature, and wind) and further  
289 found that the high RH near 100% at night (Figure S1) could enhance the emissions of PBAPs.  
290 This result is consistent with the conclusion of Elbert et al. (2007), who showed that PBAPs in a  
291 boreal forest are generally most abundant in samples collected at night when the RH is close to



292 100%. Moreover, Troutt and Levetin (2001) found that the increase in PBAP concentration was  
293 caused by the increase in basidiospores concentrations with RH, and they showed that a clear  
294 diurnal rhythm occurs and peaks at 04:00-06:00 LT. Furthermore, the number ratio (4.6 at  
295 nighttime and 4.0 at daytime) of bacterial vs fungal particles and their number concentrations  
296 increased from daytime to nighttime (Figure 2S). These results might suggest that higher RH can  
297 promote the emission of bacterial and fungal particles in boreal forests.

298

### 299 3.3 Mixing state of bacterial particles

300 Our study shows that bacterial particles are the most abundant PBAPs in the boreal forest air.  
301 Figure 6 shows that the bacterial particles frequently occurred in fine and coarse modes. Although  
302 approximately 80% of bacteria particles were externally mixed particles in the boreal forest air, we  
303 still found that 20% of bacterial particles were internally mixed particles. TEM observations show  
304 that bacterial particles were frequently internally mixed with mineral, metal, organics, and  
305 inorganic salts. We noticed that irregular mineral dust particles significantly changed the shape of  
306 the bacterial particles (Figure 13a-c). The EDS analysis shows that the internally mixed mineral  
307 particles contain certain amounts of C, O, and P in addition to Si, Al, or Ca (Figure 13a-c),  
308 suggesting that bacterial particles were coated with mineral dust particles. Patterson et al. (2016)  
309 used cryo-TEM to observe soft bacterial structures in the atmosphere, and these irregular solid  
310 mineral dust particles can transform the shape of the bacterial particles during their physical  
311 coagulation processes.

312 In this study, we found that some nanoscale metal particles were internally mixed with  
313 bacterial particles. Figure 13d-f further shows that these metals were spherical and contained Mn,



314 Si and/or Fe. As in previous studies, similar nanosize metal particles were emitted from industrial  
315 emissions or power plants instead of natural soil (Li et al., 2017). TEM observations show that  
316 these metallic particles were mainly attached to the surface of bacterial particles. Moreover, some  
317 bacterial particles were coated by inorganic salts (e.g., K-P in Figure 13g and S-rich in Figure 13i)  
318 and organics. The shape of the bacterial particles might change following the aging process during  
319 long-range transport (Figure 13), although the elemental P or its associated ionic components  
320 ( $\text{H}_2\text{PO}_4^-$  and  $\text{PO}_3^-$ ) did not change (Pratt et al., 2009). Pratt et al. (2009) detected  $\text{H}_2\text{PO}_4^-$  and  $\text{PO}_3^-$   
321 in individual cloud ice-crystal residues to identify PBAPs using aerosol time-of-flight mass  
322 spectrometry. Although one study indicates that a few mineral dust or fly ash particles contain  
323 trace inorganic P, these particles do not contain abundant organics and their number is low in the  
324 air (Zawadowicz et al., 2017).

325

### 326 **3.4 Hygroscopicity of PBAPs**

327 In this study, we conducted a hygroscopic experiment to observe the hygroscopic growth of  
328 fresh PBAPs. Before the hygroscopic experiment, an SEM analysis of the sample was performed,  
329 and it showed that bacterial and fungal spores are dominant (Figure 2a). In the hygroscopic  
330 experiment, primary bacterial and fungal spores all take up water and grow by up to 88% during  
331 hydration, and they lose water and return to the dry particle size (reduction of 83%) during  
332 dehydration (Figure 14). The growth factor of the bacterial and fungal spores is  $\sim 1.09$  at 94%  
333 based on the particle diameter change (Figure 14). These results show that fresh PBAPs have  
334 extremely weak hygroscopicity.

335 Recent studies found that fungal fragments collected in Amazon forests displayed strong



336 hygroscopic properties (China et al., 2016;China et al., 2018) and were internally mixed with  
337 certain amounts of sodium salts. However, we found weak hygroscopic growth at 1.09, whereas  
338 this value was in the range of 1.05-1.3 for bacterial and fungal spores in previous studies  
339 (Reponen et al., 1996;Lee et al., 2002). However, the result is much lower than the value of 2.31 at  
340 RH 96% for sodium salt (China et al., 2016) and 1.60 at RH 94% for ammonium sulfate (Sun et  
341 al., 2018). The comparison suggests that fresh PBAPs display extremely weak hygroscopicity and  
342 do not contain any sodium salt in the boreal forest (Figure 2a). We integrated the morphological,  
343 chemical composition and the low growth factor data of individual PBAPs and further concluded  
344 that certain hydrophilic organic species might enhance the PBAP size at higher RH. Overall, our  
345 results indicate that PBAPs from the substantial biological emissions from the Khingan Mountain  
346 boreal forest are weakly hygroscopic in nature.

347

#### 348 **4. Atmospheric implications and conclusions**

349 The TEM and SEM observations both showed that the morphology of PBAPs were unique  
350 and different from that of the sulfate, mineral, soot, organics, and metal particles in continental air.  
351 As a result, P derived from the particle EDS analysis coupled with the morphological features can  
352 be used to identify the PBAPs. In this study, we establish one full database that includes the  
353 morphology and composition of bacteria, fungi, and brochosomes, and it can be used to identify  
354 primary biological particles using single particle techniques. We estimated that the mass  
355 concentration of PBAPs, mineral dust, and remaining particles accounted for 47%, 43%, and 10%  
356 of the  $PM_{2.5-10}$  mass concentration, respectively, indicating that large boreal forests might  
357 represent a major source of PBAPs in the atmosphere. The hygroscopic experiment shows that the



358 primary bacterial and fungal particles all take up water and grow by up at 88% during hydration,  
359 and the particles lose water and return to the dry particle size (reduction of 83%) during  
360 dehydration. The growth factor of the bacterial and fungal spores is  $\sim 1.09$  at 94%, suggesting that  
361 some hydrophilic organic species might enhance the size of PBAPs at higher RH.

362 PBAPs from the natural source may have an important role in precipitation and cloud  
363 dynamics in the background areas (Prenni et al., 2009; Huffman et al., 2013). Field observations at  
364 downwind areas of the Asian continent found substantial bacteria in dust plumes (Hara and Zhang,  
365 2012). The mechanisms by which PBAPs influence mineral dust particles if they become  
366 internally mixed particles, as shown in Figure 13a-c, remain unclear. Our results indicate that  
367 significant amounts of PBAPs are emitted from the Khingan Mountain area acting as the “green  
368 ocean” (Poschl et al., 2010) in Northeast Asia, and they may have an important impact on clouds  
369 and climate in Northeast China and in the downwind North Pacific Ocean. Therefore, the  
370 modelling work required to simulate how a large number of submicron primary biological  
371 particles from boreal forests promote the atmospheric biogeochemical cycle and have a significant  
372 impact on climate by acting as CCN and IN over the large boreal forest and the downwind areas.

373



374 **Author Contributions:** WL designed the study. WL, LL, QY, LX, and HY collected  
375 aerosol particles. WL, LL, LX, YZ, BW, XD, and JZ contributed laboratory  
376 experiments and data analysis. WL prepared the manuscript with contributions from  
377 all the coauthors. BW, DH, DL, WH, DZ, PF, MY, MH, XZ, and ZS commented and  
378 edited the paper.

379

380 **Competing interests:** The authors declare no competing financial interests

381

#### 382 **Acknowledgments**

383 We appreciate Peter Hyde's comments and proofreading. This work was funded by the  
384 National Natural Science Foundation of China (9184430003, 41622504 and 41575116),  
385 Zhejiang Provincial Natural Science Foundation of China (LZ19D050001), and Zhejiang  
386 University Education Foundation Global Partnership Fund. All the data are presented in the  
387 paper.

388

389



390 **References:**

- 391 Amato, P., Ménager, M., Sancelme, M., Laj, P., Mailhot, G., and Delort, A.-M.: Microbial population in  
392 cloud water at the Puy de Dôme: Implications for the chemistry of clouds, *Atmos. Environ.*, 39,  
393 4143-4153, <https://doi.org/10.1016/j.atmosenv.2005.04.002>, 2005.
- 394 Bauer, H., Kasper-Giebl, A., Löflund, M., Giebl, H., Hitznerberger, R., Zibuschka, F., and Puxbaum, H.:  
395 The contribution of bacteria and fungal spores to the organic carbon content of cloud water,  
396 precipitation and aerosols, *Atmos. Res.*, 64, 109-119, [https://doi.org/10.1016/S0169-8095\(02\)00084-4](https://doi.org/10.1016/S0169-8095(02)00084-4),  
397 2002.
- 398 Bauer, H., Schueller, E., Weinke, G., Berger, A., Hitznerberger, R., Marr, I. L., and Puxbaum, H.:  
399 Significant contributions of fungal spores to the organic carbon and to the aerosol mass balance of the  
400 urban atmospheric aerosol, *Atmos. Environ.*, 42, 5542-5549,  
401 <https://doi.org/10.1016/j.atmosenv.2008.03.019>, 2008.
- 402 Chen, H., and Yao, M.: A high-flow portable biological aerosol trap (HighBioTrap) for rapid microbial  
403 detection, *J. Aerosol Sci.*, 117, 212-223, <https://doi.org/10.1016/j.jaerosci.2017.11.012>, 2018.
- 404 China, S., Wang, B., Weis, J., Rizzo, L., Brito, J., Cirino, G. G., Kovarik, L., Artaxo, P., Gilles, M. K.,  
405 and Laskin, A.: Rupturing of Biological Spores As a Source of Secondary Particles in Amazonia,  
406 *Environ. Sci. Technol.*, 50, 12179-12186, [10.1021/acs.est.6b02896](https://doi.org/10.1021/acs.est.6b02896), 2016.
- 407 China, S., Burrows, S. M., Wang, B., Harder, T. H., Weis, J., Tanarhte, M., Rizzo, L. V., Brito, J., Cirino,  
408 G. G., Ma, P.-L., Cliff, J., Artaxo, P., Gilles, M. K., and Laskin, A.: Fungal spores as a source of sodium  
409 salt particles in the Amazon basin, *Nat. Commun.*, 9, 4793, [10.1038/s41467-018-07066-4](https://doi.org/10.1038/s41467-018-07066-4), 2018.
- 410 Christner, B. C., Cai, R., Morris, C. E., McCarter, K. S., Foreman, C. M., Skidmore, M. L., Montross, S.  
411 N., and Sands, D. C.: Geographic, Seasonal, and Precipitation Chemistry Influence on the Abundance  
412 and Activity of Biological Ice Nucleators in Rain and Snow, *P. Natl. Acad. Sci.*, 105, 18854-18859,  
413 2008.
- 414 Denning, D. W., O'Driscoll, B. R., Hogaboam, C. M., Bowyer, P., and Niven, R. M.: The link between  
415 fungi and severe asthma: a summary of the evidence, *European Respiratory Journal*, 27, 615-626,  
416 [10.1183/09031936.06.00074705](https://doi.org/10.1183/09031936.06.00074705), 2006.
- 417 Després, V., Huffman, J. A., Burrows, S. M., Hoose, C., Safatov, A., Buryak, G., Fröhlich-Nowoisky, J.,  
418 Elbert, W., Andreae, M., Pöschl, U., and Jaenicke, R.: Primary biological aerosol particles in the  
419 atmosphere: a review, *Tellus B*, 64, 15598, [10.3402/tellusb.v64i0.15598](https://doi.org/10.3402/tellusb.v64i0.15598), 2012.



- 420 Elbert, W., Taylor, P. E., Andreae, M. O., and Pöschl, U.: Contribution of fungi to primary biogenic  
421 aerosols in the atmosphere: wet and dry discharged spores, carbohydrates, and inorganic ions, *Atmos.*  
422 *Chem. Phys.*, 7, 4569-4588, 10.5194/acp-7-4569-2007, 2007.
- 423 Fröhlich-Nowoisky, J., Pickersgill, D. A., Després, V. R., and Pöschl, U.: High diversity of fungi in air  
424 particulate matter, *P. Natl. Acad. Sci.*, 106, 12814-12819, 10.1073/pnas.0811003106, 2009.
- 425 Gabey, A. M., Gallagher, M. W., Whitehead, J., Dorsey, J. R., Kaye, P. H., and Stanley, W. R.:  
426 Measurements and comparison of primary biological aerosol above and below a tropical forest canopy  
427 using a dual channel fluorescence spectrometer, *Atmos. Chem. Phys.*, 10, 4453-4466,  
428 10.5194/acp-10-4453-2010, 2010.
- 429 Georgakopoulos, D. G., Després, V., Fröhlich-Nowoisky, J., Psenner, R., Ariya, P. A., Pósfai, M., Ahern,  
430 H. E., Moffett, B. F., and Hill, T. C. J.: Microbiology and atmospheric processes: biological, physical  
431 and chemical characterization of aerosol particles, *Biogeosciences*, 6, 721-737, 10.5194/bg-6-721-2009,  
432 2009.
- 433 Graham, B., Guyon, P., Maenhaut, W., Taylor, P. E., Ebert, M., Matthias-Maser, S., Mayol-Bracero, O.  
434 L., Godoi, R. H. M., Artaxo, P., Meixner, F. X., Moura, M. A. L., Rocha, C. H. E. D. A., Grieken, R. V.,  
435 Glosky, M. M., Flagan, R. C., and Andreae, M. O.: Composition and diurnal variability of the natural  
436 Amazonian aerosol, *J. Geophys. Res.*, 108, 4765, doi:10.1029/2003JD004049, 2003.
- 437 Hara, K., and Zhang, D.: Bacterial abundance and viability in long-range transported dust, *Atmos.*  
438 *Environ.*, 47, 20-25, 10.1016/j.atmosenv.2011.11.050, 2012.
- 439 Hu, W., Murata, K., Fukuyama, S., Kawai, Y., Oka, E., Uematsu, M., and Zhang, D.: Concentration and  
440 Viability of Airborne Bacteria Over the Kuroshio Extension Region in the Northwestern Pacific Ocean:  
441 Data From Three Cruises, *J. Geophys. Res.*, 122, 12,892-812,905, 10.1002/2017JD027287, 2017.
- 442 Hu, W., Niu, H., Murata, K., Wu, Z., Hu, M., Kojima, T., and Zhang, D.: Bacteria in atmospheric  
443 waters: Detection, characteristics and implications, *Atmos. Environ.*, 179, 201-221,  
444 <https://doi.org/10.1016/j.atmosenv.2018.02.026>, 2018.
- 445 Huffman, J. A., Treutlein, B., and Pöschl, U.: Fluorescent biological aerosol particle concentrations and  
446 size distributions measured with an Ultraviolet Aerodynamic Particle Sizer (UV-APS) in Central  
447 Europe, *Atmos. Chem. Phys.*, 10, 3215-3233, 10.5194/acp-10-3215-2010, 2010.
- 448 Huffman, J. A., Sinha, B., Garland, R. M., Snee-Pollmann, A., Gunthe, S. S., Artaxo, P., Martin, S. T.,  
449 Andreae, M. O., and Pöschl, U.: Size distributions and temporal variations of biological aerosol



450 particles in the Amazon rainforest characterized by microscopy and real-time UV-APS fluorescence  
451 techniques during AMAZE-08, *Atmos. Chem. Phys.*, 12, 11997-12019, 10.5194/acp-12-11997-2012,  
452 2012.

453 Huffman, J. A., Prenni, A. J., DeMott, P. J., Pöhlker, C., Mason, R. H., Robinson, N. H.,  
454 Fröhlich-Nowoisky, J., Tobo, Y., Després, V. R., Garcia, E., Gochis, D. J., Harris, E., Müller-Germann,  
455 I., Ruzene, C., Schmer, B., Sinha, B., Day, D. A., Andreae, M. O., Jimenez, J. L., Gallagher, M.,  
456 Kreidenweis, S. M., Bertram, A. K., and Pöschl, U.: High concentrations of biological aerosol particles  
457 and ice nuclei during and after rain, *Atmos. Chem. Phys.*, 13, 6151-6164, 10.5194/acp-13-6151-2013,  
458 2013.

459 Lee, B. U., Kim, S. H., and Kim, S. S.: Hygroscopic growth of *E. coli* and *B. subtilis* bioaerosols, *J.*  
460 *Aerosol Sci.*, 33, 1721-1723, [https://doi.org/10.1016/S0021-8502\(02\)00114-3](https://doi.org/10.1016/S0021-8502(02)00114-3), 2002.

461 Li, W., Shao, L., Zhang, D., Ro, C.-U., Hu, M., Bi, X., Geng, H., Matsuki, A., Niu, H., and Chen, J.: A  
462 review of single aerosol particle studies in the atmosphere of East Asia: morphology, mixing state,  
463 source, and heterogeneous reactions, *J. Clean. Prod.*, 112, Part 2, 1330-1349, 2016.

464 Li, W., Xu, L., Liu, X., Zhang, J., Lin, Y., Yao, X., Gao, H., Zhang, D., Chen, J., Wang, W., Harrison, R.  
465 M., Zhang, X., Shao, L., Fu, P., Nenes, A., and Shi, Z.: Air pollution–aerosol interactions produce more  
466 bioavailable iron for ocean ecosystems, *Sci. Adv.*, 3, e1601749, 2017.

467 Li, W. J., and Shao, L. Y.: Transmission electron microscopy study of aerosol particles from the brown  
468 hazes in northern China, *J. Geophys. Res.*, 114, D05202, 2009.

469 Ling, M. L., Wex, H., Grawe, S., Jakobsson, J., Löndahl, J., Hartmann, S., Finster, K., Boesen, T., and  
470 Šantl-Temkiv, T.: Effects of Ice Nucleation Protein Repeat Number and Oligomerization Level on Ice  
471 Nucleation Activity, *J. Geophys. Res.*, 123, 1802-1810, 10.1002/2017JD027307, 2018.

472 Möhler, O., DeMott, P. J., Vali, G., and Levin, Z.: Microbiology and atmospheric processes: the role of  
473 biological particles in cloud physics, *Biogeosciences*, 4, 1059-1071, 10.5194/bg-4-1059-2007, 2007.

474 Martin, S. T., Andreae, M. O., Artaxo, P., Baumgardner, D., Chen, Q., Goldstein, A. H., Guenther, A.,  
475 Heald, C. L., Mayol-Bracero, O. L., McMurry, P. H., Pauliquevis, T., Pöchl, U., Prather, K. A., Roberts,  
476 G. C., Saleska, S. R., Silva Dias, M. A., Spracklen, D. V., Swietlicki, E., and Trebs, I.: Sources and  
477 properties of Amazonian aerosol particles, *Rev. Geophys.*, 48, RG2002, 10.1029/2008rg000280, 2010.

478 May, N. W., Olson, N. E., Panas, M., Axson, J. L., Tirella, P. S., Kirpes, R. M., Craig, R. L., Gunsch, M.  
479 J., China, S., Laskin, A., Ault, A. P., and Pratt, K. A.: Aerosol Emissions from Great Lakes Harmful



- 480 Algal Blooms, *Environ. Sci. Technol.*, 52, 397-405, 10.1021/acs.est.7b03609, 2018.
- 481 Morris, C. E., Georgakopoulos, D. G., and Sands, D. C.: Ice nucleation active bacteria and their  
482 potential role in precipitation, *J. Phys. IV France*, 121, 87-103, 2004.
- 483 Patterson, J. P., Collins, D. B., Michaud, J. M., Axson, J. L., Sultana, C. M., Moser, T., Dommer, A. C.,  
484 Conner, J., Grassian, V. H., Stokes, M. D., Deane, G. B., Evans, J. E., Burkart, M. D., Prather, K. A.,  
485 and Gianneschi, N. C.: Sea Spray Aerosol Structure and Composition Using Cryogenic Transmission  
486 Electron Microscopy, *ACS Central Sci.*, 2, 40-47, 10.1021/acscentsci.5b00344, 2016.
- 487 Poschl, U.: Atmospheric aerosols: Composition, transformation, climate and health effects, *Angew.*  
488 *Chem. Int. Edit.*, 44, 7520-7540, 10.1002/anie.200501122, 2005.
- 489 Poschl, U., Martin, S. T., Sinha, B., Chen, Q., Gunthe, S. S., Huffman, J. A., Borrmann, S., Farmer, D.  
490 K., Garland, R. M., Helas, G., Jimenez, J. L., King, S. M., Manzi, A., Mikhailov, E., Pauliquevis, T.,  
491 Petters, M. D., Prenni, A. J., Roldin, P., Rose, D., Schneider, J., Su, H., Zorn, S. R., Artaxo, P., and  
492 Andreae, M. O.: Rainforest Aerosols as Biogenic Nuclei of Clouds and Precipitation in the Amazon,  
493 *Science*, 329, 1513-1516, 10.1126/science.1191056, 2010.
- 494 Posfai, M., Li, J., Anderson, J. R., and Buseck, P. R.: Aerosol bacteria over the southern ocean during  
495 ACE-1, *Atmos. Res.*, 66, 231-240, 2003.
- 496 Pratt, K. A., DeMott, P. J., French, J. R., Wang, Z., Westphal, D. L., Heymsfield, A. J., Twohy, C. H.,  
497 Prenni, A. J., and Prather, K. A.: In situ detection of biological particles in cloud ice-crystals, *Nat.*  
498 *Geosci.*, 2, 398-401, 2009.
- 499 Prenni, A. J., Petters, M. D., Kreidenweis, S. M., Heald, C. L., Martin, S. T., Artaxo, P., Garland, R. M.,  
500 Wollny, A. G., and Poschl, U.: Relative roles of biogenic emissions and Saharan dust as ice nuclei in  
501 the Amazon basin, *Nat. Geosci.*, 2, 402-405, 2009.
- 502 Rakitov, R., and Gorb, S. N.: Brochosomal coats turn leafhopper (Insecta, Hemiptera, Cicadellidae)  
503 integument to superhydrophobic state, *P. Roy. Soc. Lond. B: Bio.*, 280, 10.1098/rspb.2012.2391, 2013.
- 504 Reponen, T., Willeke, K., Ulevicius, V., Reponen, A., and Grinshpun, S. A.: Effect of relative humidity  
505 on the aerodynamic diameter and respiratory deposition of fungal spores, *Atmos. Environ.*, 30,  
506 3967-3974, [https://doi.org/10.1016/1352-2310\(96\)00128-8](https://doi.org/10.1016/1352-2310(96)00128-8), 1996.
- 507 Rissler, J., Vestin, A., Swietlicki, E., Fisch, G., Zhou, J., Artaxo, P., and Andreae, M. O.: Size  
508 distribution and hygroscopic properties of aerosol particles from dry-season biomass burning in  
509 Amazonia, *Atmos. Chem. Phys.*, 6, 471-491, 10.5194/acp-6-471-2006, 2006.



- 510 Shi, Z., Shao, L., Jones, T. P., Whittaker, A. G., Lu, S., Berube, K. A., He, T., and Richards, R. J.:  
511 Characterization of airborne individual particles collected in an urban area, a satellite city and a clean  
512 air area in Beijing, 2001, *Atmos. Environ.*, 37, 4097-4108, 2003.
- 513 Shi, Z., He, K., Xue, Z., Yang, F., Chen, Y., Ma, Y., and Luo, J.: Properties of individual aerosol  
514 particles and their relation to air mass origins in a south China coastal city, *J. Geophys. Res.*, 114,  
515 doi:10.1029/2008JD011221, 2009.
- 516 Spracklen, D. V., Bonn, B., and Carslaw, K. S.: Boreal forests, aerosols and the impacts on clouds and  
517 climate, *Philos. T. R. Soc. A.*, 366, 4613-4626, 10.1098/rsta.2008.0201, 2008.
- 518 Sun, J., Liu, L., Xu, L., Wang, Y., Wu, Z., Hu, M., Shi, Z., Li, Y., Zhang, X., Chen, J., and Li, W.: Key  
519 Role of Nitrate in Phase Transitions of Urban Particles: Implications of Important Reactive Surfaces for  
520 Secondary Aerosol Formation, *J. Geophys. Res.*, 123, 1234-1243, 10.1002/2017JD027264, 2018.
- 521 Therkorn, J., Thomas, N., Scheinbeim, J., and Mainelis, G.: Field performance of a novel passive  
522 bioaerosol sampler using polarized ferroelectric polymer films, *Aerosol Sci. Tech.*, 51, 787-800,  
523 10.1080/02786826.2017.1316830, 2017.
- 524 Tobo, Y., Prenni, A. J., DeMott, P. J., Huffman, J. A., McCluskey, C. S., Tian, G., Pöhlker, C., Pöschl,  
525 U., and Kreidenweis, S. M.: Biological aerosol particles as a key determinant of ice nuclei populations  
526 in a forest ecosystem, *J. Geophys. Res.*, 118, 10,100-110,110, 10.1002/jgrd.50801, 2013.
- 527 Troutt, C., and Levetin, E.: Correlation of spring spore concentrations and meteorological conditions in  
528 Tulsa, Oklahoma, *Int. J. Biometeorol.*, 45, 64-74, 10.1007/s004840100087, 2001.
- 529 Tunved, P., Hansson, H.-C., Kerminen, V.-M., Ström, J., Maso, M. D., Lihavainen, H., Viisanen, Y.,  
530 Aalto, P. P., Komppula, M., and Kulmala, M.: High Natural Aerosol Loading over Boreal Forests,  
531 *Science*, 312, 261-263, 10.1126/science.1123052, 2006.
- 532 Twohy, C. H., McMeeking, G. R., DeMott, P. J., McCluskey, C. S., Hill, T. C. J., Burrows, S. M.,  
533 Kulkarni, G. R., Tanarhte, M., Kafle, D. N., and Toohey, D. W.: Abundance of fluorescent biological  
534 aerosol particles at temperatures conducive to the formation of mixed-phase and cirrus clouds, *Atmos.*  
535 *Chem. Phys.*, 16, 8205-8225, 10.5194/acp-16-8205-2016, 2016.
- 536 Valsan, A. E., Priyamvada, H., Ravikrishna, R., Després, V. R., Biju, C. V., Sahu, L. K., Kumar, A.,  
537 Verma, R. S., Philip, L., and Gunthe, S. S.: Morphological characteristics of bioaerosols from  
538 contrasting locations in southern tropical India – A case study, *Atmos. Environ.*, 122, 321-331,  
539 <https://doi.org/10.1016/j.atmosenv.2015.09.071>, 2015.



540 Wittmaack, K.: Brochosomes produced by leafhoppers—a widely unknown, yet highly abundant species  
541 of bioaerosols in ambient air, *Atmos. Environ.*, 39, 1173-1180,  
542 <https://doi.org/10.1016/j.atmosenv.2004.11.003>, 2005.

543 Wittmaack, K., Wehnes, H., Heinzmann, U., and Agerer, R.: An overview on bioaerosols viewed by  
544 scanning electron microscopy, *Sci. Total Environ.*, 346, 244-255,  
545 <https://doi.org/10.1016/j.scitotenv.2004.11.009>, 2005.

546 Wu, L., Li, X., Kim, H., Geng, H., Godoi, R. H. M., Barbosa, C. G. G., Godoi, A. F. L., Yamamoto, C.  
547 I., de Souza, R. A. F., Pöhlker, C., Andreae, M. O., and Ro, C. U.: Single-particle characterization of  
548 aerosols collected at a remote site in the Amazonian rainforest and an urban site in Manaus, Brazil,  
549 *Atmos. Chem. Phys.*, 19, 1221-1240, [10.5194/acp-19-1221-2019](https://doi.org/10.5194/acp-19-1221-2019), 2019.

550 Yue, S., Ren, H., Fan, S., Wei, L., Zhao, J., Bao, M., Hou, S., Zhan, J., Zhao, W., Ren, L., Kang, M., Li,  
551 L., Zhang, Y., Sun, Y., Wang, Z., and Fu, P.: High Abundance of Fluorescent Biological Aerosol  
552 Particles in Winter in Beijing, China, *ACS Earth Space Chem.*, 1, 493-502,  
553 [10.1021/acsearthspacechem.7b00062](https://doi.org/10.1021/acsearthspacechem.7b00062), 2017.

554 Zawadowicz, M. A., Froyd, K. D., Murphy, D. M., and Cziecho, D. J.: Improved identification of  
555 primary biological aerosol particles using single-particle mass spectrometry, *Atmos. Chem. Phys.*, 17,  
556 7193-7212, [10.5194/acp-17-7193-2017](https://doi.org/10.5194/acp-17-7193-2017), 2017.

557 Zhang, D., Murata, K., Hu, W., Yuan, H., Li, W., Matsusaki, H., and Kakikawa, M.: Concentration and  
558 Viability of Bacterial Aerosols Associated with Weather in Asian Continental Outflow: Current  
559 Understanding, *Aerosol Sci. Engin.*, 1-12, [10.1007/s41810-017-0008-y](https://doi.org/10.1007/s41810-017-0008-y), 2017.

560 Zhou, S., Zhao, H., Peng, J., Hong, Q., Xiao, K., Shang, Y., Lu, S., Zhang, W., Wu, M., Li, S., Yu, S.,  
561 Wang, W., and Wang, Q.: Size distribution of *Platanus acerifolia* allergen 3 (Pla a3) in Shanghai  
562 ambient size-resolved particles and its allergenic effects, *Atmos. Environ.*, 198, 324-334,  
563 <https://doi.org/10.1016/j.atmosenv.2018.10.060>, 2019.

564



*Figure Captions*

**Figure 1** Location of the sampling site in a boreal forest of the Lesser Khingan Mountain in Northeast China. The map source is Google Earth.

**Figure 2** Low magnification SEM and TEM images of individual particles collected from the forest air. (a) low magnification SEM image of bacterial (red arrow) and fungal particles (green color); (b) SEM image of a single bacterial particle; (c) low magnification TEM image of bacteria aggregations and single bacterial particles; (d) low magnification TEM image of single bacterial particles and secondary sulfate (S-rich) particles; (e) TEM image of mineral dust particle (f) TEM image of an organic matter (OM) particle; and (g) TEM image of S-OM coating internally mixed with a soot particle. The color in (a) (also in the following figures) was artificially painted on the original SEM images.

**Figure 3** Number fractions of different types of particles in different size bins and their total number fraction (a); and number fractions of primary biological aerosol particles (PBAPs) and non-PBAPs during the day and night (b). The number of analyzed particles is listed above each column.

**Figure 4** TEM image of one rod-like bacterial particle and EDS spectra of bacterial inclusions and other parts.

**Figure 5** TEM images showing different shapes of bacterial particles.

**Figure 6** TEM/EDS showing the morphology and composition of various fungal particles. (a) Rod-like fungi particle; (b) fungi particle with bubbles; (c) fungi particle with bubbles; and (d) EDS spectrum showing the composition of fungi particles.

**Figure 7** Color SEM images showing the shape, size, and surface properties of fungal particles. Size represents the diameter of fungal particles. (a-d) Surfaces of three rod-like fungal particles with a layer of strips. The green-colored particles are conidia, and the attached pink particles on the



conidia are fragments from other unknown biological particles. (e-f) Surfaces of two fungal particles with bubbles. The green particles are fungi spores, and the attached red part on the spores is a fragment from other unknown biological particles. The color is artificially modified through the original SEM.

**Figure 8** TEM images of brochosomes and the composition of (a) a single brochosome and brochosome aggregations; (b) high-resolution TEM image showing the inner structure of one brochosome; (c) EDS spectrum showing the chemical composition of the brochosomes.

**Figure 9** Color SEM images of brochosomes. (a) Single brochosome and their aggregations. Some brochosomal particles are associated with primary biological species. (b) High-resolution SEM image showing the surface properties of the brochosomal particles.

**Figure 10** TEM images showing the morphology of the primary biological particles. (a) One elongated particle with thorns; (b) one circular particle; (c-d) two elongated particles; and (e) one spindle particle

**Figure 11** Color SEM image showing the morphology and surface properties of three elongated biological particles.

**Figure 12** Size distribution of PBAPs and mass concentration of daily  $PM_{2.5}$ . (a) Number fraction (right y-axis) and size distribution (left y-axis) of three types of primary biological particles. (b) Daily mass concentrations of  $PM_{2.5}$  and  $PM_{10}$  and their ratio during the sampling period

**Figure 13** Internally mixed bacteria particles observed by TEM. (a-c) Internal mixture of mineral and bacteria; (d-f) internal mixture of metal and bacteria; (g) internal mixture of inorganic salts and bacteria; (h) internal mixture of organics and bacteria; and (i) internal mixture of S-rich salts and bacteria.

**Figure 14** Hygroscopic growth of the primary biological particles on the silicon wafer collected at night. All the particles confirmed by SEM are bacteria and fungi. The up arrows (i.e., RH) represent hydration, and the down arrows represent dehydration.



**Figure 1** Location of the sampling site in a boreal forest of the Lesser Khingan Mountain in Northeast China. The map source is Google Earth.

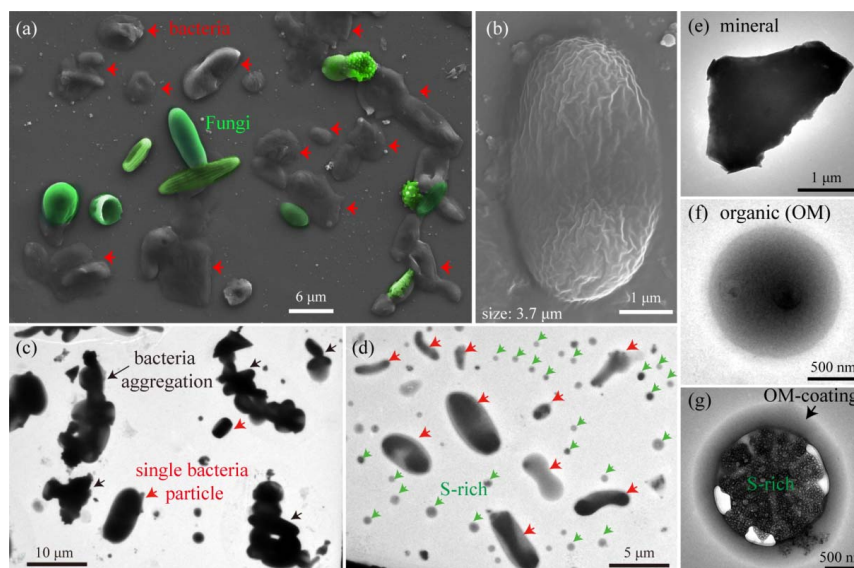


**Figure 2** Low magnification SEM and TEM images of individual particles collected from the forest air. (a) low magnification SEM image of bacterial (red arrow) and fungal particles (green color); (b) SEM image of a single bacterial particle; (c) low magnification TEM image of bacteria aggregations and single bacterial particles; (d) low magnification TEM image of single bacterial particles and secondary sulfate (S-rich) particles; (e) TEM image of mineral dust particle (f) TEM image of an organic matter



(OM) particle; and (g) TEM image of S-OM coating internally mixed with a soot particle. The color in (a) (also in the following figures) was artificially painted on the original SEM images.

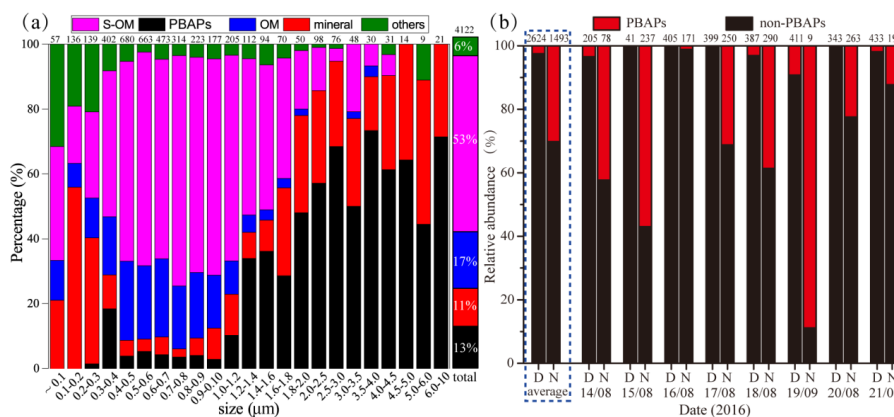


**Figure 3** Number fractions of different types of particles in different size bins and their total number fraction (a); and number fractions of primary biological aerosol particles (PBAPs) and non-PBAPs during the day and night (b). The number of analyzed particles is listed above each column.

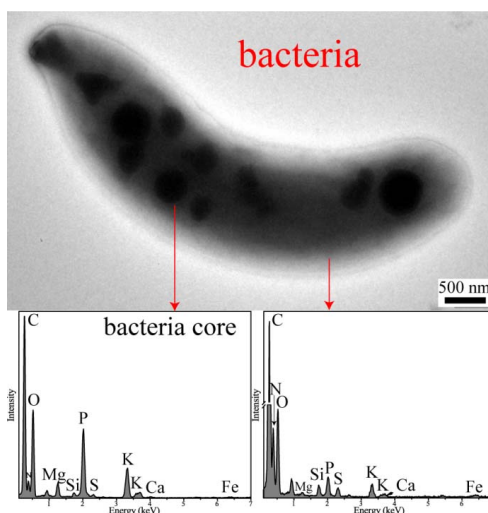


**Figure 4** TEM image of one rod-like bacterial particle and EDS spectra of bacterial inclusions and other parts.

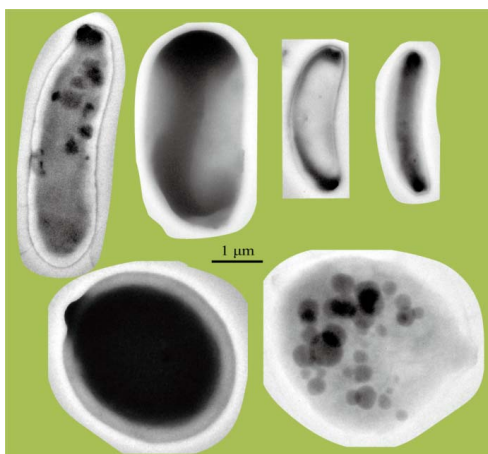


**Figure 5** TEM images showing different shapes of bacterial particles.

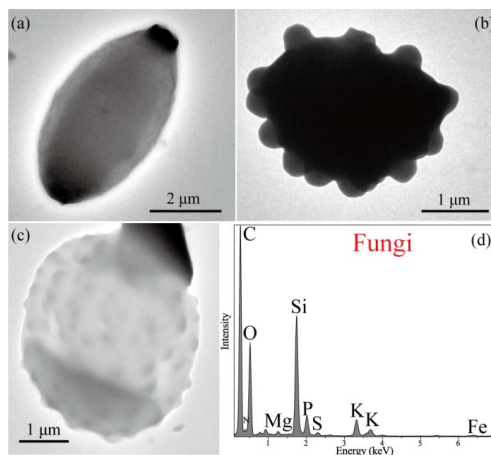


**Figure 6** TEM/EDS showing the morphology and composition of various fungal particles. (a) Rod-like fungi particle; (b) fungi particle with bubbles; (c) fungi particle with bubbles; and (d) EDS spectrum showing the composition of fungi particles.

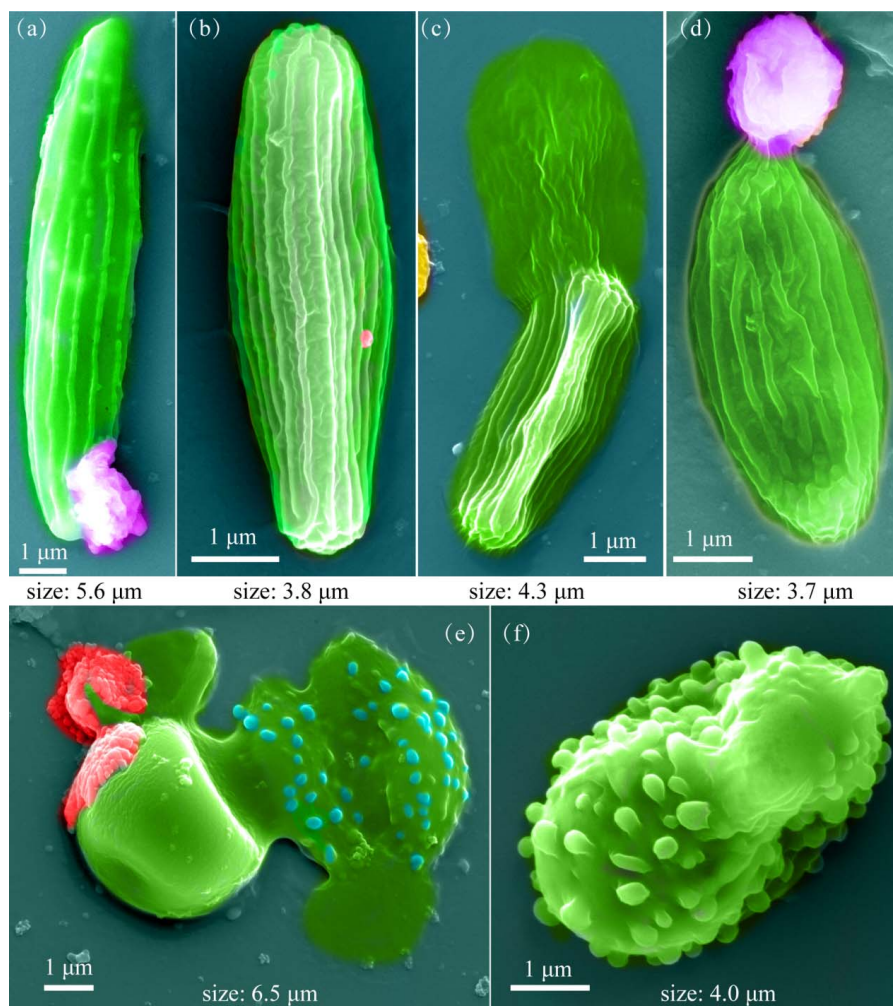


**Figure 7** Color SEM images showing the shape, size, and surface properties of fungal particles. Size represents the diameter of fungal particles. (a-d) Surfaces of three rod-like fungal particles with a layer of strips. The green-colored particles are conidia, and the attached pink particles on the conidia are fragments from other unknown biological particles. (e-f) Surfaces of two fungal particles with bubbles. The green particles are fungi spores, and the attached red part on the spores is a fragment from other unknown biological particles. The color is artificially modified through the original SEM.

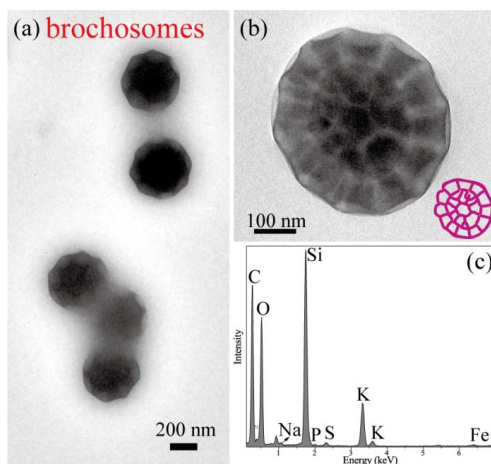


**Figure 8** TEM images of brochosomes and the composition of (a) a single brochosome and brochosome aggregations; (b) high-resolution TEM image showing the inner structure of one brochosome; (c) EDS spectrum showing the chemical composition of the brochosomes.

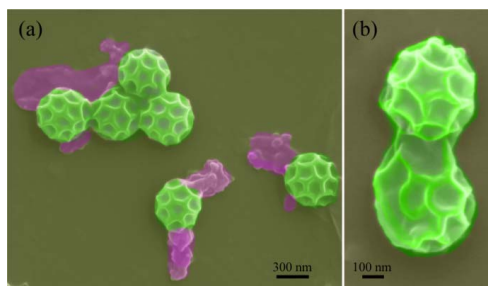


**Figure 9** Color SEM images of brochosomes. (a) Single brochosome and their aggregations. Some brochosomal particles are associated with primary biological species. (b) High-resolution SEM image showing the surface properties of the brochosomal particles.

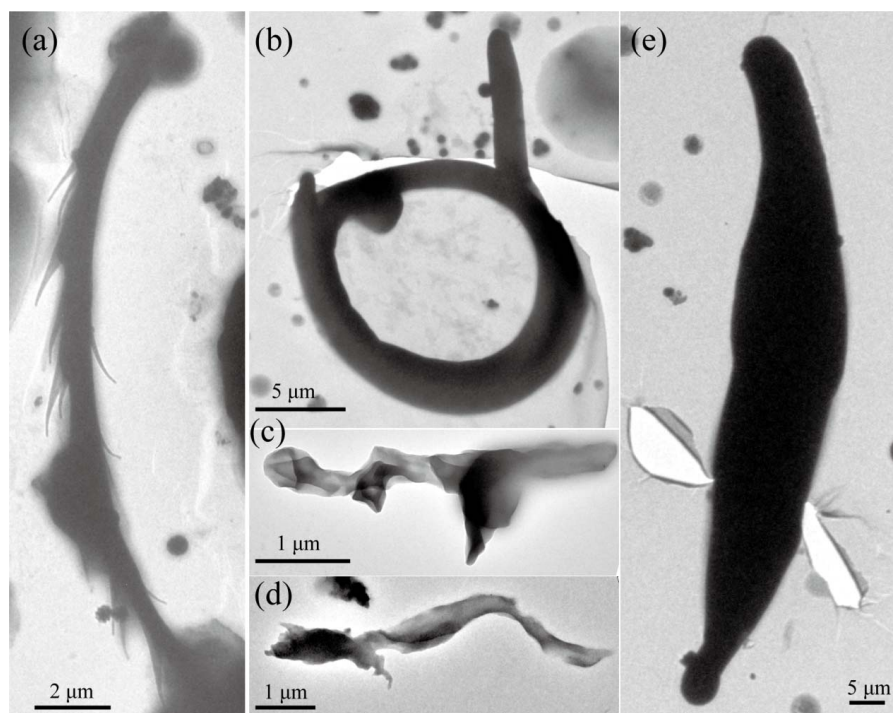


**Figure 10** TEM images showing the morphology of the primary biological particles. (a) One elongated particle with thorns; (b) one circular particle; (c-d) two elongated particles; and (e) one spindle particle



**Figure 11** Color SEM image showing the morphology and surface properties of three elongated biological particles.

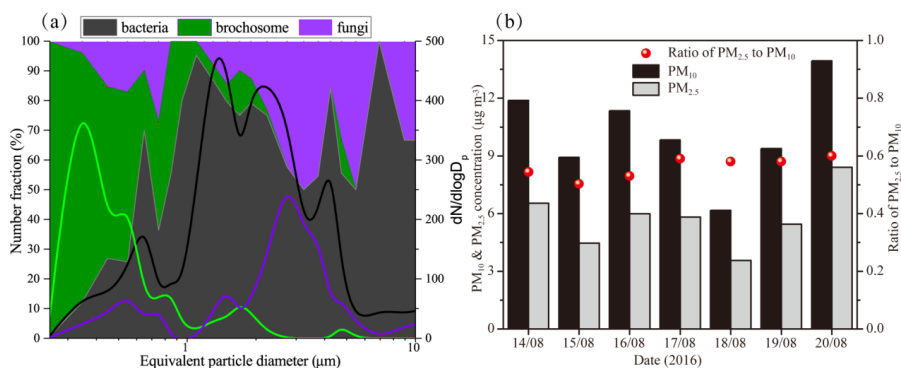


**Figure 12** Size distribution of PBAPs and mass concentration of daily  $PM_{2.5}$ . (a) Number fraction (right y-axis) and size distribution (left y-axis) of three types of primary biological particles. (b) Daily mass concentrations of  $PM_{2.5}$  and  $PM_{10}$  and their ratio during the sampling period

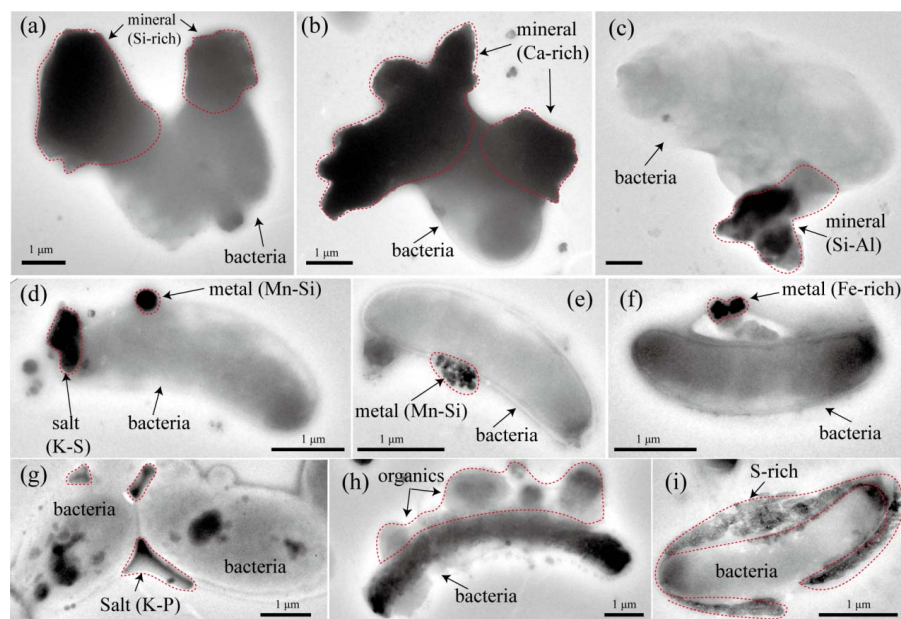


**Figure 13** Internally mixed bacteria particles observed by TEM. (a-c) Internal mixture of mineral and bacteria; (d-f) internal mixture of metal and bacteria; (g) internal mixture of inorganic salts and bacteria; (h) internal mixture of organics and bacteria; and (i) internal mixture of S-rich salts and bacteria.

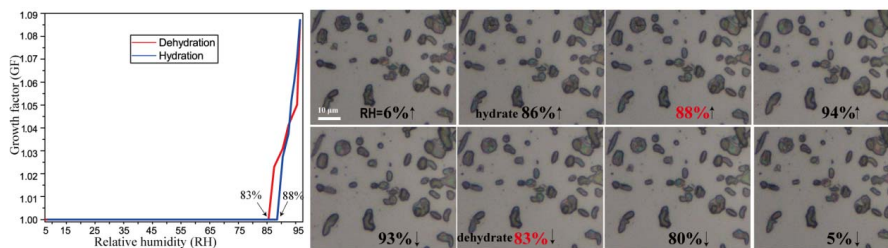


**Figure 14** Hygroscopic growth of the primary biological particles on the silicon wafer collected at night. All the particles confirmed by SEM are bacteria and fungi. The up arrows (i.e., RH) represent hydration, and the down arrows represent dehydration.